*remote sensing*

MDPI

*Article*

# In-Season Crop Mapping with GF-1/WFV Data by Combining Object-Based Image Analysis and Random Forest

**Qian Song [1], Qiong Hu [1], Qingbo Zhou [1], Ciara Hovis [2], Mingtao Xiang [1], Huajun Tang [1] and Wenbin Wu [1,*]**

[1] Key Laboratory of Agricultural Remote Sensing (AGRIRS), Ministry of Agriculture/Institute of Agricultural Resources and Regional Planning, Chinese Academy of Agricultural Sciences, Beijing 100081, China; songqian01@caas.cn (Q.S.); huqiongnky@163.com (Q.H.); zhouqingbo@caas.cn (Q.Z.); xiangmt_caas@163.com (M.X.); tanghuajun@caas.cn (H.T.)

[2] Center for System Integration and Sustainability, Michigan State University, East Lansing, MI 48824, USA; hoviscia@msu.edu

* Correspondence: wuwenbin@caas.cn; Tel.: +86-10-82105070

Received: 17 October 2017; Accepted: 16 November 2017; Published: 17 November 2017

**Abstract:** Producing accurate crop maps during the current growing season is essential for effective agricultural monitoring. Substantial efforts have been made to study regional crop distribution from year to year, but less attention is paid to the dynamics of composition and spatial extent of crops within a season. Understanding how crops are distributed at the early developing stages allows for the timely adjustment of crop planting structure as well as agricultural decision making and management. To address this knowledge gap, this study presents an approach integrating object-based image analysis with random forest (RF) for mapping in-season crop types based on multi-temporal GaoFen satellite data with a spatial resolution of 16 meters. A multiresolution local variance strategy was used to create crop objects, and then object-based spectral/textural features and vegetation indices were extracted from those objects. The RF classifier was employed to identify different crop types at four crop growth seasons by integrating available features. The crop classification performance of different seasons was assessed by calculating F-score values. Results show that crop maps derived using seasonal features achieved an overall accuracy of more than 87%. Compared to the use of spectral features, a feature combination of in-season textures and multi-temporal spectral and vegetation indices performs best when classifying crop types. Spectral and temporal information is more important than texture features for crop mapping. However, texture can be essential information when there is insufficient spectral and temporal information (e.g., crop identification in the early spring). These results indicate that an object-based image analysis combined with random forest has considerable potential for in-season crop mapping using high spatial resolution imagery.

**Keywords:** crop mapping; in-season; object-based classification; Random Forest

## 1. Introduction

The timely availability of the spatial distribution of crop types is required for statistical and economic purposes as well as agrarian policy actions related to subsidy payments or implementation of agro-environmental measurements [1,2]. Understanding the dynamic progress of the composition and spatial structure of mosaicking crops is critical for a diversity of agricultural monitoring activities (e.g., crop acreage estimation, yield modeling, harvest operations schedules and greenhouse gas mitigation) [3–5]. Recently, there has been an increasing demand for delivering information on the spatial distribution and dynamics of different crop types as early as possible, as in-season the crop

maps are curtailed when taken as input to crop area forecasting, hazard prediction, or water use calculations [6]. However, high accuracy and early identifications of crop distribution across an entire growing period is challenging [7,8]. Since traditional agricultural statistics on crop acreages are usually provided by the end of the season or later, in-season agricultural production managers lack necessary information about the current year's crops [9,10]. Alternatively, remote sensing satellites, owing to their synoptic and repetitive nature, have proven to be an effective means for mapping and monitoring crop extent [11–13].

The spectral characteristics recorded by the sensors provide a reliable basis for crop mapping. Crop leaf pigment, leaf water and canopy structure all have a strong effect on spectral response. However, the inherent spectral variability of crop types is frequently influenced by local weather or farmer decisions. Specifically, different crops in the same region may share similar spectral signatures, while the same crop types may present different spectral signatures in different locations [14,15]. Fortunately, each crop has a specific crop calendar with well-defined planting times as well as unique seasonal growth and development rhythms, resulting in variation among apparent spectral reflecting performance within the crop-growing season [16]. Therefore, temporal features are extremely necessary for accurate crop classification. However, the tradeoff between spatial resolution and temporal coverage makes it difficult to acquire data at simultaneously high levels [17].

The Moderate Resolution Imaging Spectroradiometer (MODIS) data can be used in long time-series research at regional or global scales, but often suffer from high mixtures of crop types due to coarse spatial resolution (i.e., >250 m). Alternatively, spatial resolution of a few tens of meters, such as Landsat data, can describe spatial details of land cover well, but Landsat-like data are hardly used to capture changes in crop phenology and growth due to low temporal repeat cycles and frequent cloud contamination. Thus, crop mapping based on satellite data desperately requires high-quality spatial and temporal data, particularly in China where agricultural landscapes are complex with a diversity of cropping systems and small field sizes [18]. New sensors, such as Chinese GaoFen and overseas Sentinel-2A sensor, were designed for data enhancement to offer unprecedented perspectives on land cover/use and vegetation [19–22]. These new missions revisit the same area more frequently (every four or ten days) [23,24]. These data's fine spatial resolution, global coverage and relatively fine temporal resolution make them of great utility for mapping crop distribution [25,26]. In fact, such high spatial resolution time series with multiple bands and possible derivations contribute large volumes of data that present significant challenges for in-season crop mapping.

For the challenges due to crop variability and pixel heterogeneity, traditional pixel-based classification methods are unable to incorporate the detailed spatial information, which limits their application mainly in the regions where crop fields are fragmented with high spectral variability [27,28]. To overcome the "salt-and-pepper" effect, object-based approaches have been increasingly implemented in remote-sensed image analysis [29,30]. Since object-based methods can avoid being affected by spectral similarity between different crops or crop mosaicking variability, techniques based on objects become a more useful approach to map crop types [31]. In addition to the reflectance signal captured by the sensors, textural features can correspond to crop consistency and canopy structure [32,33]. Object-based methods can calculate these textural features, which describe spatial and structural attributes of crops at the object-based scale. However, conventional supervised classifiers (e.g., maximum likelihood method) are inefficient for determining the separabilities of a large volume of features (such as spectral, temporal, texture and vegetation indices) at an object-scale under complex cropping conditions.

Recently developed nonparametric machine learning algorithms, i.e., support vector machine (SVM) and random forest (RF), provide effective tools to identify different land cover classes, as they are not constrained by the assumption that the input parameters are normally distributed [34–36]. RF classifier has been given increasing attention with regards to crop mapping [37–39]. The RF classifier has been proven to be stable and relatively efficient to yield overall accuracy levels that are either comparable to or better than other classifiers such as decision trees, neural networks and SVM [40].

Additionally, RF can not only deal with a large volume of spectral, temporal and texture features (even those that are highly correlated), but it can also measure feature importance and enable automatic generation of a structured knowledge, which may be a promising method for crop classification when using high spatial resolution images. Therefore, the performance of a combination of RF approaches with object-based image analysis for crop mapping has garnered much attention [25,41,42]. However, few studies have paid much attention to producing the early seasonal crop type maps for decision-maker management and mapping crop seasonal dynamics based on new "two high resolution" satellite data.

This paper aims to address the knowledge gap for the timely production of in-season crop maps to detail the composition and spatial distribution of crops and their seasonal changes during crop growing stages. A combined object-based image analysis with random forest for mapping in-season crop types (OBRFIC) is introduced to produce the multiple crop type maps from early spring to autumn. To demonstrate the utility of this method, multiple temporal Chinese GaoFen satellite no. 1 Wide Field-of-View camera (GF-1 WFV) data located in Beian City in northeast China from 2014 were employed. We first segmented the GF-1 WFV imageries and tested the optimal segmentation parameters for crop objects. Then, object-based spectral, temporal, textural features and vegetation indices were extracted. Ten different feature combinations were designed and their performance was assessed. Finally, we mapped the in-season crop types and ranked feature importance with RF. Compared to post-season crop mapping, this work provides the advantage of using multiple seasonal features for mapping in-season crop types during crop growth to support agricultural production management.

## 2. Study Area and Datasets

### *2.1. Study Area*

The study area is located to the west of Beian City, Heilongjiang, China (Figure 1). It covers approximately 4647.83 km$^2$ between 47.54°–48.57° N in latitude and 126.26°–127.50° E in longitude. Beian City is an agriculturally dominated region and is also the leading soybean production region. It is characterized by a flat terrain and a cold temperate regional climate. Winters are long and frigid, and summers are short and cool, with an annual average temperature ranging from −0.6 °C to 2.7 °C. Annual precipitation averages 500–700 mm, with precipitation occurring mainly in summer. The major crop types in this region are soybeans and corn, accounting for two-thirds of the total cropland area [43]. In addition, there is some rice and spring wheat cultivation in the study area. Due to the limited accumulated heat and sunshine, the four major crops are cultivated once each year and have relatively stable calendars (Figure 2). In general, soybean and corn are usually planted in mid- to late-May. The harvest dates of these two crops are different, ranging from late September to as late as mid-October. Wheat is sowed earliest and harvested earliest among the four crops. Rice are transplanted in early June and harvested in late September, experiencing a relatively long growing period.

### *2.2. GF-1 WFV Data*

The GF-1 WFV sensor data were chosen for in-season crop mapping in this study because of their high spatial resolution and temporal repeat interval. Launched on 26 April 2013, GF-1 is the first optical satellite of the "Chinese high-resolution satellite" program. The GF-1 WFV sensor has four spectral channels, i.e., blue (450–520 nm), green (520–590 nm), red (630–690 nm) and near infrared (770–890 nm). GF-1 WFV image has a spatial resolution of 16 m and swath width of 800 km with four cameras combined, as well as a 4-day revisit cycle. Four GF-1 WFV images in 2014 were downloaded from the China Centre for Resource Satellite Data and Application [44]. Considering the availability of cloud-free images and crop calendar, four GF-1 WFV scenes, acquired in early spring (no crop cover stage; 24 April 2014), spring (green-up stage; 24 May 2014), summer (growing peak stage; 25 July 2014), and autumn (harvest stage; 24 September 2014) were selected to characterize the

variations of crop planting pattern across time. These data cover the key growing phases of targeted crops and were of good quality. All those images were georeferenced to the UTM WGS84 (zone 52N-WGS84) projection system. Atmospheric corrections were implemented to these images using Fast Line-of-sight Atmospheric Analysis of Spectral Hypercubes (FLAASH) module in ENVI 5.1 software.

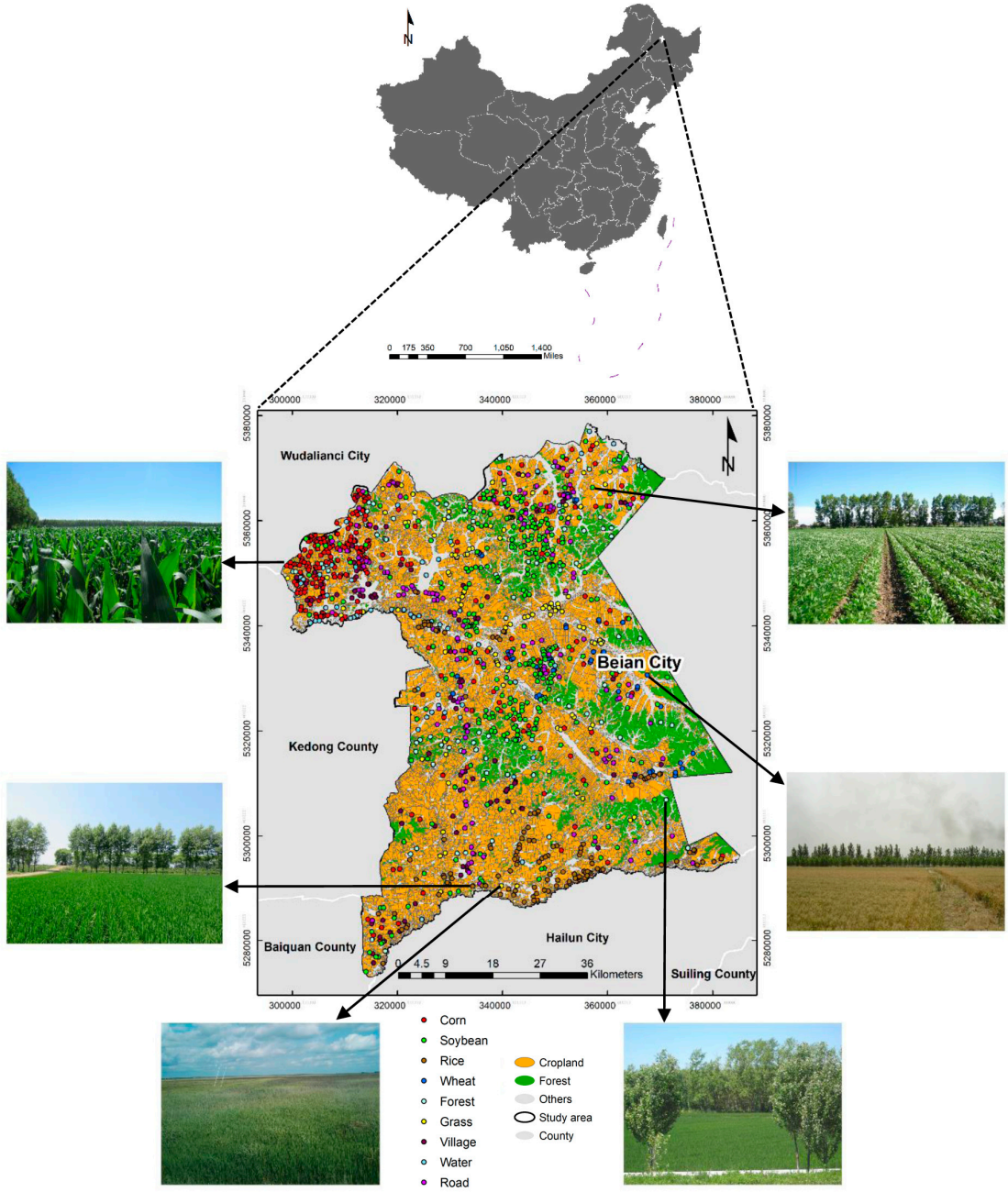


**Figure 1.** Location of the study area and the sampling points in summer.

## 2.3. In-Season Sample Data

To build the RF classification model and assess the accuracy of the in-season crop maps, extensive field surveys were carried out across different crop growth period. A detailed survey schedule was designed according to the crop calendar. Sample plots were chosen according to the adequate number of crop samples to capture the existing land system, the size of the field and their accessibility. Only the field with area greater than 256 $m^2$ (16 m $\times$ 16 m) was selected as the sample plot. A distance of

no less than 1 km was chosen as the sampling interval so as to guarantee their spatial homogeneity and representativeness of intra-class variations. A total of 1777 sample plots was collected and were distributed throughout the whole study area (Figure 1), including 1121 crop samples (located in cropland corn, soybeans, rice and wheat) and 656 non-crop classes (mainly village, road, water, forest and grassland) samples. Then, the field investigations were monthly conducted to collect crop types for four stages, i.e., they are respectively no crop cover stage, green-up stage, growing peak stage and harvested stage. The specific dates for surveying sampling point data were assigned at the end of every month and these seasons are characterized by different vegetation coverage type. The locations of sample plots were first recorded by GPS and then digitized as points over the available fine resolution GF-1 WFV images. Then, these sample plots were randomly divided into 70% and 30% for the training and validation points, respectively. The numbers of training and validation samples for each crop type are listed in Table 1.

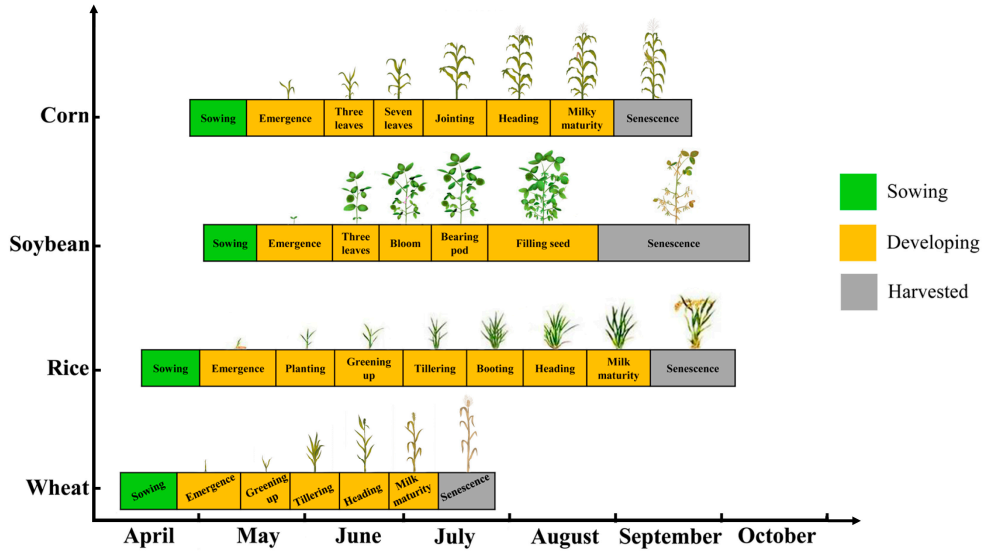


**Figure 2.** Crop calendars in Beian City, Heilongjiang Province.

**Table 1.** Targeted crop types and associated number of training and validation samples at different crop growing phrases in 2014.

| Survey Date | Crop Types | Samples | Training Samples | Validation Samples |
|---|---|---|---|---|
| 20 April | Cropland | 1121 | 789 | 332 |
| | Others | 656 | 516 | 140 |
| 20 May | Wheat | 68 | 53 | 15 |
| | Non-wheat | 1053 | 736 | 317 |
| | Others | 656 | 516 | 140 |
| 20 July | Corn | 415 | 275 | 140 |
| | Soybean | 474 | 334 | 140 |
| | Rice | 164 | 126 | 38 |
| | Wheat | 68 | 53 | 15 |
| | Others | 656 | 516 | 140 |
| 20 September | Corn | 415 | 275 | 140 |
| | Soybean | 474 | 334 | 140 |
| | Rice | 164 | 126 | 38 |
| | Wheat-other | 68 | 53 | 15 |
| | Others | 656 | 516 | 140 |

## 3. Methodology

The workflow of OBRFIC schedule involved three parts: (1) image segmentation to create the meaningful entities; (2) object-based feature extraction to select and build a training database for different season; (3) running the trained RF for each season and assessing the crop maps. The flow diagram in Figure 3 outlines the main processing and analysis steps, which are described in detail in the following sub-sections.

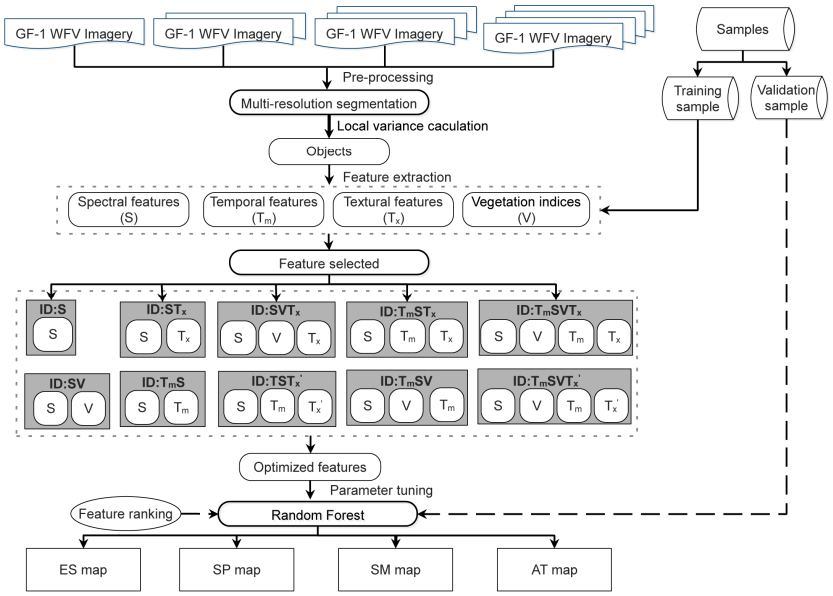


**Figure 3.** Flow diagram of the processing and analysis steps. ID group of feature scenario; S spectral feature; $T_x$ texture feature; $T_m$ temporal feature; $T_x$' in-season texture feature; ES in the early spring season; SP in the spring season; SM in the summer season; AT in the autumn season.

### *3.1. Overview of In-Season Crop Classification*

The in-season classification scheme based on OBRFIC is implemented to produce a series of crop maps for early prediction during the crop developing period. The four seasons and their identified crop types are summarized in Table 2. While land preparation was occurring, non-crop class was identified during plowing and tilling period. Thus, cropland was preliminarily discriminated from other land cover types (village areas, natural vegetation, water bodies, etc.) in early spring (ES). Then some of cropland became colonized by wheat. The extraction of the spatial distribution of wheat was performed in spring based on the combination of two GF-1 imageries acquired in April and May (SP). In summer, corn, soybean and rice with high biomass developed as the dominant green crop, while wheat was mostly senescent. The summer crop distribution was extracted by combining three available imageries in summer (SM). In autumn, summer crops were senescent, while wheat had been reaped. We combined all the key growing-stage imageries ranging from early spring to harvested stage to understand ongoing crop type changes in the region (AT). Based on OBRFIC approach, various experiments were carried out for the dynamic crop development:

- A multiresolution algorithm was used for image segmentation and the appropriate segmentation scale and the parameters associated with heterogeneity criterion were selected according to local variance;
- Evaluation on the performance of the features for different crop types according to their types (spectral reflectance, texture, temporal features and vegetation indexes);
- Analysis of the contribution of different feature types to the classification accuracy.

**Table 2.** Four different seasons and its mapping crop types.

| In-Season ID | Period of Mapping | Targeted Types |
|---|---|---|
| ES | Early spring | Cropland/Others |
| SP | Spring | Non-wheat/Wheat/Others |
| SM | Summer | Corn/Soybean/Rice/Wheat/Others |
| AT | Autumn | Corn/Soybean/Rice/Wheat-other/Others |

### *3.2. Image Segmentation*

The segmentation of GF-1WFV imageries includes two steps: (1) the delimitation of homogeneous crop objects using a multiresolution segmentation algorithm; (2) the selection of optimal segmentation parameter combination based on local variance (LV).

The first step to identify homogeneous crop objects is image segmentation. Objects, basic processing units, were generated using a multiresolution segmentation algorithm implemented in the eCognition Developer 8.7 platform (Trimble GeoSpatial Imaging), which is a bottom-up region-merging technique [45]. The outcome of the segmentation process for producing homogeneous objects is controlled though specifications and weighting of a scale factor and a heterogeneity criterion. The scale factor is indirectly related to the average size of the detected objects. The heterogeneity criterion controls the merging decision process and is determined by two mutually exclusive properties (i.e., color and shape). Shape is composed of two equally exclusive properties: smoothness and compactness. However, land use/cover types differ in spectral and spatial characteristics as well as various shape and structure, the inherent properties of land use/cover and landscape pattern impact on the scale levels for individual land cover types in order to match structures in the real world. Therefore, the multiresolution segmentation is an optimization procedure for the average heterogeneity and produces highly homogeneous image objects so that the subsequent classification process can be greatly simplified and the mapping accuracy can be significantly improved [46].

A local variance strategy was used here for optimizing segmentation. To do so, we firstly set the different segmentation scales ranging from 1 to 100 with an increment rate of 1. In addition, the shape parameters were set as 0.1, 0.3, 0.5, 0.7 and 0.9, respectively. Additionally, the segmentation performance of different parameter combinations was assessed by the Estimation of Scale Parameter (ESP) tool. The fundamental principle of ESP is to select the segmentation scales based on the Rate of Change (ROC) curve for the calculated Local Variance (LV) of object heterogeneity at various scales [47]. The scales corresponding to the peaks of ROC curves were deemed as the potentially optimal segmentation scales at the specific shape parameters. The segmentation results of different parameter combinations were visually examined whether the image objects matched the boundaries well.

### *3.3. Feature Extraction*

Four types of variables were considered: temporal ($T_m$), spectral (S), textural features ($T_x$) and vegetation indexes (V). Several variables were calculated from multi-temporal GF-1 WFV images (4 seasons). Mean blue, green, red and near-infrared spectral features were computed from the values of all pixels forming an object, showing information related to leaf pigment and vegetation status [48,49]. The textural features related to crop structure, soil background and planting patterns, including gray-level co-occurrence matrix (GLCM) correlation, dissimilarity and entropy, were calculated from GF-1 WFV bands (blue band to near infrared band) [50,51]. The texture features were calculated within the object. These textural features provided information on the pixels organization that is complementary to spectral information. Four vegetation indices, such as Normalized Difference Vegetation Index (NDVI), Enhanced Vegetation Index (EVI), Ratio Vegetation Index (RVI) and Redness Index (RI) derived from GF-1 wavebands, were calculated during the crop growing periods. These indices have been widely used in crop monitoring and they have enhanced the information of spectral reflectance. To evaluate the relative usefulness of spatio-temporal features of GF-1 WFV for

in-season crop identification, a series of feature scenarios were devised in which different combinations of feature type were tested as input to the classifier. A complete list of feature scenarios and used variables is given in Table 3.

- S: The spectral features from a single image per season were taken as input. Only four available spectral bands of each scene were selected.
- $ST_x'$: The spectral bands and texture features acquired from a single image were taken as input. Four available spectral bands (4 features) and GLCM correlation, GLCM dissimilarity, and GLCM entropy from each band (12 features) acquired in specific season were selected. This experiment represents the case where spatio-spectral feature type information is employed for crop identification.
- SV: In addition to spectral features, NDVI, EVI, RVI and RI from GF-1 WFV data acquired in specific season were taken as input to enhance the spectral information. This experiment represents the case where multiple spectral information but little temporal information and non-spatial information are employed for crop identification.
- $SVT_x'$: Along with the spatio-spectral features from a single image, vegetation indices were taken as input. This experiment represents the case where multiple spectral information but little temporal information and spatial information are employed for crop identification.
- $T_mS$: Multi-temporal available spectral features collected during the crop present growth stages were taken as input. This experiment represents the traditional "multiple-dates" approaches. It is a case of employing multiple temporal information but little spectral information (without spectral enhancement, lack of vegetation indices) and non-spatial information for crop identification.
- $T_mST_x$: Multi-temporal spectral and multi-temporal texture features were taken as the input. For each available date, the four bands and 12 texture features were selected. This experiment represents the cases of employing multiple spectral, multiple temporal and multiple texture information for crop identification.
- $T_mST_x'$: Multi-temporal spectral and in-season texture features were taken as the input. Only 12 texture features were extracted from the special spectral bands acquired in present season. This experiment represents the case of employing multiple temporal, multiple spectral but little texture information to enhance the present information on crop structure and planting pattern for crop identification.
- $T_mSV$: Multi-temporal spectral features and vegetation indices were taken as input. This experiment represents the case of employing multiple temporal information and multiple spectral information for crop identification.
- $T_mSVT_x$: The available spatio-temporal spectral and vegetation indices collected during the crop present growth stages were taken as input.
- $T_mSVT_x'$: Only the specific texture features were added into the multi-temporal spectral features and vegetation indices datasets.

**Table 3.** Groups of input variables for in-season crop classification. Numbers in dark color means the group is included in the selection.

| Feature Scenario | ES | | | | SP | | | | SM | | | | AT | | | |
|---|---|---|---|---|---|---|---|---|---|---|---|---|---|---|---|---|
| | **S** | **$T_m$** | **$T_x$** | **V** | **S** | **$T_m$** | **$T_x$** | **V** | **S** | **$T_m$** | **$T_x$** | **V** | **S** | **$T_m$** | **$T_x$** | **V** |
| **S** | 4 | | | | 4 | | | | 4 | | | | 4 | | | |
| **$ST_x'$** | 4 | | 12 | | 4 | | 12 | | 4 | | 12 | | 4 | | 12 | |
| **SV** | 4 | | | 4 | 4 | | | 4 | 4 | | | 4 | 4 | | | 4 |
| **$SVT_x'$** | 4 | | 12 | 4 | 4 | | 12 | 4 | 4 | | 12 | 4 | 4 | | 12 | 4 |
| **$T_mS$** | | | | | 8 | 2 | | | 12 | 3 | | | 16 | 4 | | |
| **$T_mST_x$** | | | | | 8 | 2 | 24 | | 12 | 3 | 36 | | 16 | 4 | 48 | |
| **$T_mST_x'$** | | | | | 8 | 2 | 12 | | 12 | 3 | 12 | | 16 | 4 | 12 | |
| **$T_mSV$** | | | | | 8 | 2 | | 8 | 12 | 3 | | 12 | 16 | 4 | | 16 |
| **$T_mSVT_x$** | | | | | 8 | 2 | 24 | 8 | 12 | 3 | 36 | 12 | 16 | 4 | 48 | 16 |
| **$T_mSVT_x'$** | | | | | 8 | 2 | 12 | 8 | 12 | 3 | 12 | 12 | 16 | 4 | 12 | 16 |

A set of accuracy metrics including Misclassification Error Rate (MER) and F-score values were used to evaluate the performances of different feature scenario. MER, defined as the total proportion of incorrectly classified fields, was derived from the confusion matrix to assess the accuracy of crop maps in spatial location. The F-score is a per category measure that gives equal importance to the errors of omission and commission and corresponds to the harmonic mean of producer's accuracy (PA) and user's accuracy (UA). For each crop type, a class-wise accuracy measure ranges from 0 to 1, among which value 1 indicates the best result and value 0 indicate the worst.

To decrease the classification error, the classification model was repeated five times. The results were averaged by five random selections of training and validation samples to avoid the accidental errors due to the low representativeness of one-time sampling.

### *3.4. Random Forest Classification*

In this study, the RF algorithm was implemented and trained using version 3.2.2 of the 64-bit version of R in order to identify the relative useful features to conduct in-season crop classification and evaluate feature importance. RF was chosen because it has produced more accurate mapping results in land cover classification studies compared to other classifiers [52].

RF is an ensemble classification algorithm and consists of a group of tree-based classifiers [34,53]. Each tree is obtained from bootstrapping, an equiprobable random selection technique with replacement. The RF trees are built without pruning and by randomly selecting at each node a subset of input variables. The forest of classification trees is built by performing an individual learning algorithm that splits the input features into subsets based on the value of Mean Decrease Accuracy (MDA, the difference in prediction accuracy before and after permutation of the interested variable) or Gini coefficient. At each node in the trees, a random subset of the predictor variables is used to identify the most efficient split. Thus, the result is an ensemble of low bias and high variance regression trees, where the final predictions are derived by averaging the predictions of the individual trees. An internal unbiased estimate of the generalization error and confusion matrix was also generated to assess the RF model accuracy. A RF classifier based on MDA was widely used to assess the performance of features.

The critical steps of RF classification are the selection of the number of predictors at each decision tree node split (mtry) and the number of decision trees to run (ntree) [52]. The mtry parameter was set to the square root of the total number of input features within different feature scenarios (see Table 3), and the ntree parameter was set to a relatively high number (set as 1000) for each feature scenarios to allow for convergence of the Out-Of-Bag (OOB) error statistic since values larger than the default (500) are known to have little influence on the overall classification accuracy [34,51,54]. The RF model was constructed using a set of field data that was randomly divided 70%/30% for training and testing, and examined by using 10-fold cross-validation to optimize classification performance. Additionally, based on the results of feature ranking, the importance of features for different seasons were analyzed and compared to evaluate how spectral, vegetation indices, temporal and textural features impact crop classification accuracies.

## 4. Results

### *4.1. The Optimal Segmentation Scale of Crop Type*

Figure 4 shows the potentially optimal segmentations scales for different land cover types were 30, 60 and 90, where the local variances changed abruptly. At each scale peak, the segmented objects visually match with geographic entity and characteristics for the different land cover types. After the segmentation, the objects at different scale levels respond to different landscape types, as scales always related to the resolution of remote sensing data and landscape patterns. After visual comparison between before- and after-segmentation images, we found these scales reflect three levels of image objects of GF-1 WFV at 16 m spatial resolution in agriculturally dominated regions: (1) crop fields with a clear boundary at scale parameter of 30, (2) blocks of artificial surface corresponding to the

scale parameter of 60, and (3) the broadest land cover classes (e.g., forest) as depicted by their rough and uneven texture of crowd structure, corresponding to scale parameter of 90. Therefore, 30 was deemed as the optimal segmentation scale for crop type, which was expected to produce high-accuracy crop maps.

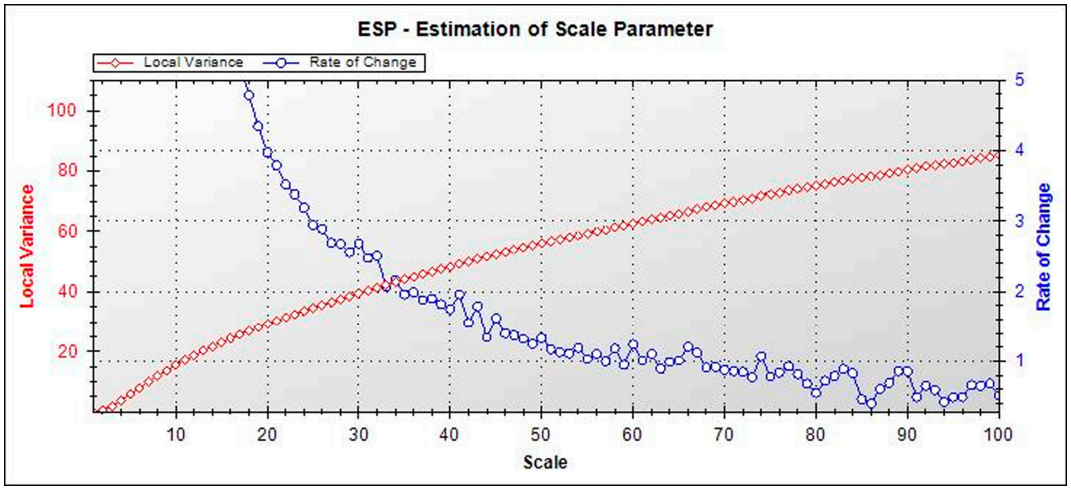


**Figure 4.** Local variance and its rate of change graph calculated by the ESP tool.

Besides the scale of segmentation, shape parameter also impacts the performance of segmentation, especially for geographic entities possessing regular shapes (Figure 5). Cropland, as the main geographic entity type in study area, was monitored at spatial resolution of 16 m (Figure 5a). A quantitative test was implemented, and the box plot shows that the value of local variance accelerated with the increase of the shape factor (Figure 5e). The local variance noticeably increased by 62.5% as shape grew from 0.1 to 0.9, with the step size of 0.1. Additionally, the highest local variance occurred at the shape value of 0.9, while the lowest one happened at the shape value of 0.1. Increasing the shape parameter results in a significant discrepancy in the performance of segmentation (Compared Figure 5c with Figure 5d). Thus, the optimum image objects are segmented at shape parameter of 0.1. From the above analysis, scale and shape parameters should be optimized for crop field to obtain the best segmentation.

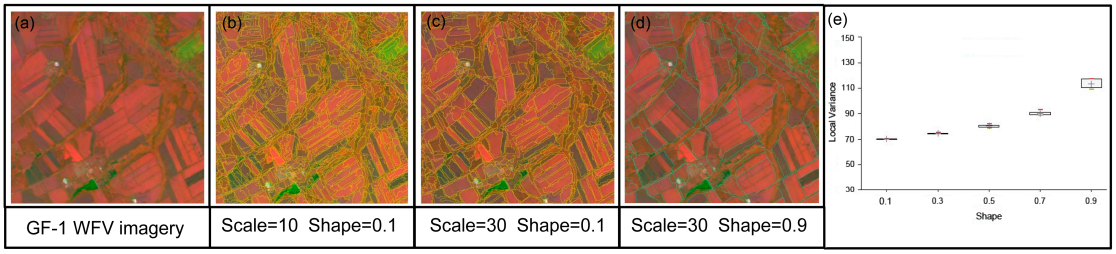


**Figure 5.** Image segmentation at two scale levels and with two shape parameters: (**a**) Standard false color composites (band rank: near-infrared, red, and green) of GF-1 WFV layer stack imagery; (**b**) Segmentation at scale value of 10 and shape parameter value of 0.1; (**c**) Segmentation at scale value of 30 and shape parameter value of 0.1; (**d**) Segmentation at scale value of 30 and shape parameter value of 0.9; (**e**) Box plot depicting local variance (LV) against the different shape parameter settings at a scale value of 30 of the multiresolution segmentation algorithm.

### *4.2. Performances of Different Feature Subspaces on Crop Classification*

By combining the spectral, temporal, spatial features and vegetation indices of the input data, the average MERs of 10 scenarios for each season are presented in Figure 6. The overall performance of ten feature groups achieves acceptable accuracies, suggesting that the features directly acquired from GF-1 remote sensed images are capable of distinguishing in-season crop types. However, all MERs are lower than 0.30. It is also observed that MERs significantly decrease as spatio-spectral information increases, and MER ranges from 28.96% to 8.16%. The single spectral information (S) has the worst performance and produces the lowest overall accuracies during the crop developing and harvest stages. After adding texture (compared S with $ST_x$), the improvements in performance are not remarkable and MERs just decrease by 0.51–1.12%, as a result of providing information on the organization of objects that is complementary to spectral information, however extra texture information does not work in ES. The vegetation indices, the efficient enhancement of spectral features, are the most beneficial information in crop classification when available spectral information is limited, and $SVT_x'$ work best using single temporal data for in-season crop mapping with an MER of 12.17 to 21.26%. When more temporal features are available in crop growing periods, MERs decease dramatically to 2.89–13.37% (compared $T_mS$ with S). Additionally, multi-temporal vegetation indices are able to notably improve accuracies. However, multi-temporal textures are less helpful than in-season textures (compared $T_mST_x$ with $T_mST_x'$), especially in the lager volume of feature scenarios (compared $T_mSVT_x$ with $T_mSVT_x'$). In contrast, Scenario $T_mSVT_x'$ works best for each season, with an MER of 8.16 to 12.17% ($SVT_x'$ in ES is equal to $T_mSVT_x'$ for in-season crop mapping during the early spring). The same feature composition during different crop developing seasons indicates the time-scale scalability to the other growing seasons.

| | ES | SP | SM | AT |
|---|---|---|---|---|
| S | 15.01 | 14.39 | 28.96 | 20.32 |
| STx' | 15.80 | 13.27 | 27.78 | 19.81 |
| SV | 12.91 | 14.16 | 21.85 | 19.71 |
| SVTx' | 12.17 | 12.40 | 21.26 | 17.76 |
| TmS | | 11.50 | 15.59 | 9.54 |
| TmSTx | | 12.55 | 20.66 | 11.63 |
| TmSTx' | | 12.52 | 18.00 | 9.61 |
| TmSV | | 10.20 | 11.93 | 8.31 |
| TmSVTx | | 10.30 | 13.21 | 9.08 |
| TmSVTx' | | 10.13 | 11.42 | 8.16 |

**Figure 6.** Cross-validated MERs using different feature sets for RF classifiers.

The different sensibility of in-season crops was measured using scenario $T_mSVT_x'$ based on average F-score (Figure 7). These dynamic changes in the F-score mirror the occurrence of phenological events and the appearance of crop developing throughout the crop growing seasons. The summer crops (corn, soybean and rice) yield the best classification in season AT, with the average F-score of greater-than 86.00%. Due to extra temporal and in-season texture features, the discrimination between the pairwise crop types was facilitated by the fact that differences of crop status are larger between late summer and autumn than for early summer. For instance, the capacity of identification for corn has an increasing F-score value of 6.16% in autumn; the F-score value already achieves a desired average value of 90.23% for soybean in summer; there is a remarkable improvement of F-score for rice in autumn, with an increase value of 9.57%. Conversely, the decrease of the F-score value, provided for wheat, is founded in Season SM, with an average decrease of 1.85%. Because the earlier sowing ahead of other summer crops, wheat is in early development in spring but close to senescing in summer. Thus, the spring date is more feasible to discriminate wheat and is helpful to optimize the spatio-temporal collection schedule.

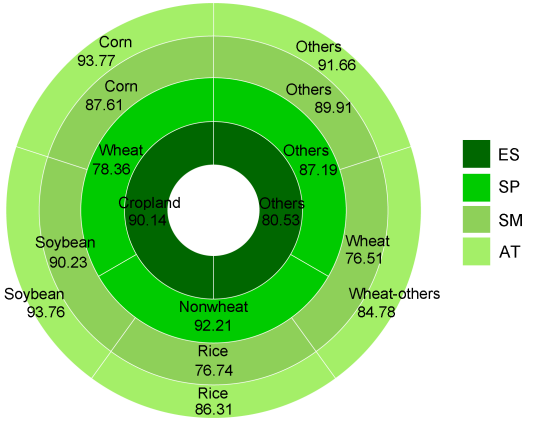


**Figure 7.** Circular plots representing the class-wise accuracy (F-score) of the RF classifier for Scenario $T_mSVT_x'$. ES in the early spring season; SP in the spring season; SM in the summer season; AT in the autumn season.

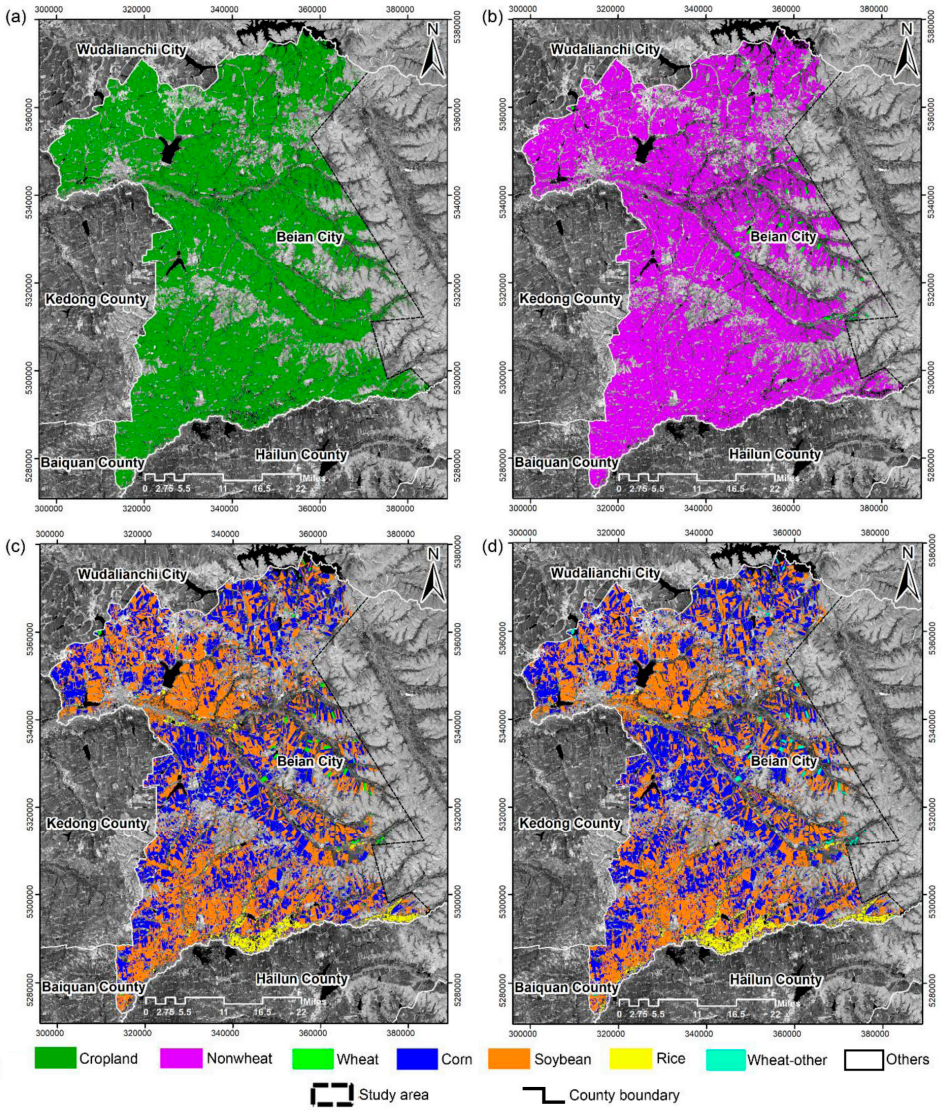


**Figure 8.** In-season crop maps derived from RF at TST feature subspace. (**a**) ES; (**b**) SP; (**c**) SM; (**d**) AT. ES in the early spring season; SP in the spring season; SM in the summer season; AT in the autumn season.

### *4.3. In-Season Crop Mapping*

Figure 8 presents in-season crop maps obtained via OBRFIC, of which the overall accuracies average over 87.00% (Table 4). The different seasons differ not only in the crop extraction but also in the error structure of the in-season maps. Cropland is firstly distinguished in early spring with an overall accuracy of 87.73% and a kappa coefficient of 0.7421 (Figure 8a). Cropland is classified with PA and UA values of approximately 90.00%, while the PA and UA values for the non-cropland class are under 86.00%. The wheat already shows green cover during spring with the result that the wheat class is further separated from cropland by using early spring and spring imagery (Figure 8b). This is mapped with an overall accuracy of 91.26%, reaching a kappa coefficient of 0.8263. Several vegetation indices related to crop vegetation vigor in early summer, plus in-season texture features, were combined to discriminate these fields. Nearly 92.38% of the non-wheat class is correctly labeled in spring season, which is attributed either to emergency stage or to bare soil in this period. The mapping result of SM is shown in Figure 8c with an overall accuracy of 87.88% and a kappa coefficient of 0.8305, distinguishing corn, soybean, rice, and senescent wheat. However, both producer's accuracy (97.14%) and user's accuracy (64.15%) of the wheat class in summer are slightly lower than the one in spring (PA: 97.22%, UA: 66.04%). The overall accuracy also slightly increases to 91.72% after adding the spatio-temporal information in autumn, demonstrating that this season is decisive for the success of the general crop identification. All the summer crop types have their highest classification accuracy, especially rice which occupies the watercourses.

**Table 4.** Classification accuracy for in-season crop mapping.

| Season ID | Classification Type | UA (%) | PA (%) |
|---|---|---|---|
| ES | Cropland | 90.86 | 89.05 |
| | Others | 82.95 | 85.60 |
| | Overall accuracy = 87.73% | | |
| | Kappa coefficient = 0.7421 | | |
| **Season ID** | **Classification Type** | **UA (%)** | **PA (%)** |
| SP | Non-wheat | 92.38 | 92.44 |
| | Wheat | 66.04 | 97.22 |
| | Others | 88.76 | 86.09 |
| | Overall accuracy = 91.26% | | |
| | Kappa coefficient = 0.8263 | | |
| **Season ID** | **Classification Type** | **UA (%)** | **PA (%)** |
| SM | Corn | 85.81 | 89.39 |
| | Soybean | 89.22 | 90.85 |
| | Rice | 77.98 | 78.23 |
| | Wheat | 64.15 | 97.14 |
| | Others | 93.21 | 86.98 |
| | Overall accuracy = 87.88% | | |
| | Kappa coefficient = 0.8305 | | |
| **Season ID** | **Classification Type** | **UA (%)** | **PA (%)** |
| AT | Corn | 90.55 | 97.65 |
| | Soybean | 94.01 | 93.18 |
| | Rice | 81.75 | 91.15 |
| | Wheat-others | 73.59 | 95.12 |
| | Others | 95.54 | 87.99 |
| | Overall accuracy = 91.72% | | |
| | Kappa coefficient = 0.8839 | | |

## 5. Discussion

In-season crop mapping is difficult to characterize using the traditional classification methods due to complex crop planting patterns and dynamic crop developing status. The proposed in-season crop mapping strategy (OBRFIC) offers the advantage of characterizing the seasonal crop distribution based on the optimized feature subset. Overall, our in-season classification results achieved desired accuracies. These good results mean that the crop maps could potentially be incorporated into a range of environmental models to predict how crop productivity may respond to unfavorable growing conditions during the current growing season.

We evaluated the performance of different segmentations in agriculturally dominated region. Previous studies have shown that, the multi-resolution segmentation, scale parameter is a key factor for obtaining the best segmentation results [11]. According to the local variances, it greatly affected the size of objects. For the crop category, a large number of small objects are acceptable but undesired because textural characters are always subject to a high level of variability, resulting in the homogeneity of objects decreasing with scale. Additionally, an excessive number of objects may increase the risk that part of a given crop field, which contains the same crop type, are mislabeled thereby affecting overall crop identification [42]. We also paid much attention to the influence of shape parameter on the segmentation in this agriculturally dominated region. Visually, larger shape parameters failed to delimit crop field borders, since segmentation errors stem from boundaries not being clear or fields not being wide enough between crops. In the other words, increasing the shape parameter meant that the segmented objects were no longer well aligned with the crop field boundaries. Thus, the combination of the optimal scale and shape parameters for segmentation shows great potential for some regular shape structures like cropland. However, in reality this optimal segmentation was not very far off from the combination that was used in this study area, which is also affected by crop structure and fragmentation.

For the performance of different feature scenarios, the results indicated that the spectral features are fundamental for in-season crop classification, and temporal features extracted from high resolution time series significantly improves the classification accuracy relative to the case of using a single image, which is also consistent with the findings of the previous studies [55–59]. Ideally, each feature would provide extra information and improve classification accuracy. Nevertheless, high correlations between the variables and information redundancy undermine classification accuracy when all features are used. Thus, $T_mSVT_x$' performed best by contrast. Additionally, this study evaluated what information is the most important for mapping in-season crops. For example, spectral diversity or enhancement of the spectral information (e.g., adding vegetation indices) is more helpful for extracting the wheat spatial distribution than temporal features due to the earlier development. The other summer crops, by contrast, are more dependent on the multi-temporal information, resulting in sharing similar crop calendar. However, the optimal feature scenario shown in this study is a combination of spectral, temporal, in-season texture information and vegetation indices, and it is hard to determine which feature type makes a greater contribution to the high crop accuracies.

We ranked the importance of the top 40% of all in-season features to test the contribution of the improved classification accuracy (Figure 9). In the early spring, GLCM correlation feature extracted from the near-infrared band in the early spring performed similarly as EVI, RVI and NDVI (Figure 9a). This indicates that textural features provide information on the organization of objects that is complementary to spectral information, which is consistent with the findings of other studies [14]. Similarly, the pattern of features in spring and multi-temporal vegetation indices occupied the importance top-rankings, with the in-season textures being more useful than those extracted from early spring data (Figure 9b). When the majority of summer crops have high vegetation vigor, RI is the most beneficial feature in crop classification, and it works best in the summer image (Figure 9c). The spectral feature extracted from the green band in summer is the most efficient texture feature, which can be attributed to the increase of MSE when feature scenarios lack in-season textures. When a large volume of features was taken as input, multi-temporal spectral and vegetation indices play an

important role in improvement of accuracy (Figure 9d). However, in-season textures, which were extracted based on September imagery, were absent in top ranking. In contrast, GLCM correlation feature, respectively extracted from the green band in spring and near-infrared band in early spring, still work well for desiccated vegetation or crop harvested in autumn. In general, the texture features contributed relatively little due to different crop calendars. The period where texture features were least influential was the one possessing the autumn period. In this period, spectral and temporal features contributed the most.

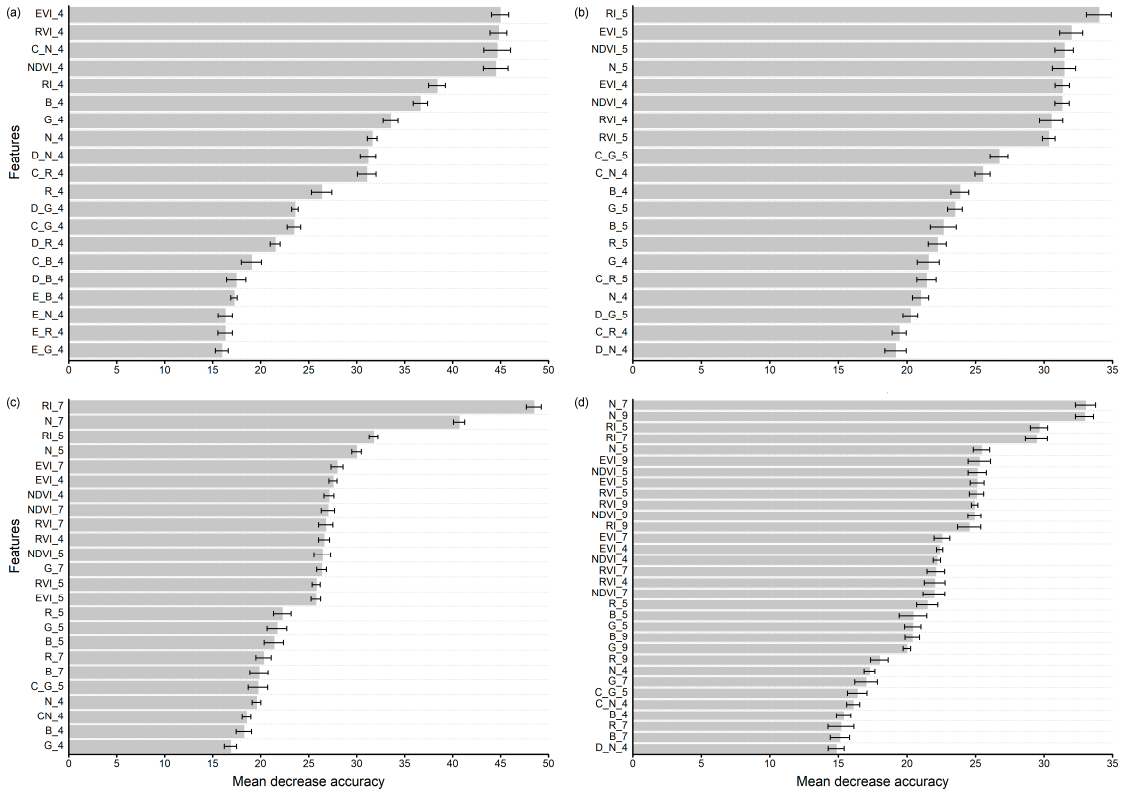


**Figure 9.** Importance of RF feature sets for in-season crop mapping at different crop growth seasons: (**a**) ES; (**b**) SP; (**c**) SM; (**d**) AT. B blue spectral band; G green spectral band; R red spectral band; N near-infrared spectral band; E gray-level co-occurrence matrix entropy; D gray-level co-occurrence matrix dissimilarity; C gray-level co-occurrence matrix correlation; 4 features extracted from the early spring imagery; 5 features extracted from the spring imagery; 7 features extracted from the summer imagery; 9 features extracted from the autumn imagery; ES in the early spring season; SP in the spring season; SM in the summer season; AT in the autumn season.

The tested OBRFIC approach performs with very good accuracy and promises high flexibility. Additionally, this approach shows great potential for early stage crop identification. For instance, wheat can be identified in spring with the highest accuracy, while the acceptable accuracy of soybean can be obtained in summer. However, classification errors are still inevitable during the different crop-growing stages. In ES, the acceptable omission error of cropland is partly attributable to spectral cross-correlation between grassland and cropland covered by crop residuals. Second, during the emergence period of wheat, its weak spectral signature due to low-vegetation cover limits the ability to differentiate between wheat and grassland, although the vegetation indices are helpful in spring. In SM, soybeans were partly classified as corn in the southwest of the study area and grassland was partly classified as rice. This is because soybean and corn, as well as rice and grassland, have similar seasonal and spectral behavior resulting in respective misclassifications. When the OBRFIC is applied to seasonal GF-1/WFV imagery, the larger feature sets weaken the interclass spectral similarities and

high intraclass spectral variability. The combination of object-based and RF increases the robustness of the mapping approach in each monitoring stage. In the presented research, the OBRFIC approach was employed to classify the in-season crop types, and the classification accuracy and certainty remained stable when additional features were used and crop types became complex.

Several factors potentially affected the results of this proposed approach. First, the number of cloud-free images and the date that correspond to crop phonological phrases influenced the quality of in-season classifications. Although the temporal resolution with GF-1 WFV data was substantially finer than other data (e.g., Landsat data), it is still difficult to obtain dense GF-1 WFV time series due to cloud contamination. Only having four clear observations introduces some uncertainty. A second limitation is the determination of segmentation parameters. A multiresolution local variance strategy has inherent instability and depends on the spatial resolution of the imagery and the a priori knowledge. Segmentation evaluation metrics, such as a modification of the Global Score, should be tested with this method to make the segmentation reproducible and less subjective [60]. Third, it is well known that using multi-source data can improve crop classification accuracy, as different information can capture crop characteristics from alternative perspectives. Thus, the combination of optical and Synthetic Aperture Radar data, such as Sentinel-1/2 data, is expected to improve the accuracies of in-season crop maps in the future.

## 6. Conclusions

This paper presented an in-depth study on in-season crop mapping using an approach of integrating object-based image analysis with random forest (RF) based on multi-season GF-1 WFV data. Four crop maps for different seasons in Beian City of Heilongjiang were produced and were assessed by the field observation data. Results showed an overall accuracy of each crop map extracted from early spring to autumn is more than 87% for 2014. These seasonal crop maps described the dynamics of composition and the spatial extent of crops across different seasons as well as the progress of crop growth. Such in-season crop extent information is particularly essential for regional agricultural decision making, such as structural adjustment of agricultural planting.

Key findings and conclusions relevant for in-season crop mapping are listed below:

- The map in the fourth season has the highest accuracy since it has the largest number of features and thus contains more useful information for classification. Therefore, for multiple-season crop mapping, more attention should be paid to the early seasons that may suffer from the insufficient information.
- Texture can be essential information for crop mapping when there is insufficient spectral and temporal information at the beginning of crop-growing period, whereas in-season texture helps increase the chance for mature crop classification, not only in addition to multi-temporal spectral information, but also avoiding redundancy and maximizing the classification accuracy.
- Even though we focus on the Beian City in 2014, our methods can be extended to other years for in-season crop monitoring since this robust approach possesses of the time-scale scalability. In addition, future work could address the issues on how to use multi-source finer spatial resolution data to improve the quality and timeliness of in-season crop mapping.

**Acknowledgments:** This study was financially supported by the National Key Research and Development Program of China (2017YFD0300201). Special thanks are also due to C. Atzberger and four anonymous reviewers for their constructive recommendation and insightful suggestions on this paper writing. The authors would like to thank the fellows at the Remote Sensing Technology Center, Heilongjiang Academy of Agriculture Sciences, for supporting the essential field investigation and crop samples.

**Author Contributions:** Qian Song, Wenbin Wu, Huajun Tang and Qingbo Zhou proposed the idea; Qian Song, Qiong Hu, and Mingtao Xiang conceived and designed the experiments; Qian Song performed the experiments; Qian Song and Qingbo Zhou analyzed the data; Qian Song, Ciara Hovis and Qiong Hu wrote the paper.

**Conflicts of Interest:** The authors declare no conflict of interest.

## References


1. Mkhabela, M.; Bullock, P.; Raj, S.; Wang, S.; Yang, Y. Crop yield forecasting on the Canadian prairies using MODIS NDVI data. *Agric. For. Meteorol.* **2011**, *151*, 385–393. [CrossRef]
2. Ozdogan, M. The spatial distribution of crop types from MODIS data: Temporal unmixing using independent component analysis. *Remote Sens. Environ.* **2010**, *114*, 1190–1204. [CrossRef]
3. Wardlow, B.D.; Egbert, S.L.; Kastens, J.H. Analysis of time-series MODIS 250 m vegetation index data for crop classification in the U.S. Central Great Plains. *Remote Sens. Environ.* **2007**, *108*, 290–310. [CrossRef]
4. Villa, P.; Bresciani, M.; Bolpagni, R.; Pinardi, M.; Giardino, C. A rule-based approach for mapping macrophyte communities using multi-temporal aquatic vegetation indices. *Remote Sens. Environ.* **2015**, *171*, 218–233. [CrossRef]
5. Wu, W.B.; Yu, Q.Y.; Peter, V.H.; You, L.Z.; Yang, P.; Tang, H.J. How could agricultural land systems contribute to raise food production under global change. *J. Integr. Agric.* **2014**, *13*, 1432–1442. [CrossRef]
6. Villa, P.; Stroppiana, D.; Fontanelli, G.; Azar, R.; Brivio, P. In-season mapping of crop type with optical and x-band sar data: A classification tree approach using synoptic seasonal features. *Remote Sens.* **2015**, *7*, 12859–12886. [CrossRef]
7. Kontgis, C.; Schneider, A.; Ozdogan, M. Mapping rice paddy extent and intensification in the Vietnamese Mekong River Delta with dense time stacks of Landsat data. *Remote Sens. Environ.* **2015**, *169*, 255–269. [CrossRef]
8. Gao, F.; Anderson, M.C.; Zhang, X.; Yang, Z.; Alfieri, J.G.; Kustas, W.P.; Mueller, R.; Johnson, D.M.; Prueger, J.H. Toward mapping crop progress at field scales through fusion of Landsat and MODIS imagery. *Remote Sens. Environ.* **2017**, *188*, 9–25. [CrossRef]
9. Conrad, C.; Fritsch, S.; Zeidler, J.; Rücker, G.; Dech, S. Per-field irrigated crop classification in arid central Asia using SPOT and ASTER data. *Remote Sens.* **2010**, *2*, 1035–1056. [CrossRef]
10. Song, X.; Potapov, P.V.; Krylov, A.; King, L.; Di Bella, C.M.; Hudson, A.; Khan, A.; Adusei, B.; Stehman, S.V.; Hansen, M.C. National-scale soybean mapping and area estimation in the United States using medium resolution satellite imagery and field survey. *Remote Sens. Environ.* **2017**, *190*, 383–395. [CrossRef]
11. Singha, M.; Wu, B.F.; Zhang, M. Object-based paddy rice mapping using Hj-1A/B data and temporal features extracted from time series MODIS NDVI data. *Sensors* **2017**, *17*, 10. [CrossRef] [PubMed]
12. Biradar, C.M.; Thenkabail, P.S.; Noojipady, P.; Li, Y.; Dheeravath, V.; Turral, H.; Velpuri, M.; Gumma, M.K.; Gangalakunta, O.R.P.; Cai, X.L.; et al. A global map of rainfed cropland areas (GMRCA) at the end of last millennium using remote sensing. *Int. J. Appl. Earth Obs.* **2009**, *11*, 114–129. [CrossRef]
13. Pan, Y.; Li, L.; Zhang, J.; Liang, S.; Zhu, X.; Sulla-Menashe, D. Winter wheat area estimate from MODIS-EVI time series using the crop proportion phenology index. *Remote Sens. Environ.* **2012**, *119*, 232–242. [CrossRef]
14. Peña-Barragán, J.M.; Ngugi, M.K.; Plant, R.E.; Six, J. Object-based crop identification using multiple vegetation indices, textural features and crop phenology. *Remote Sens. Environ.* **2011**, *115*, 1301–1316. [CrossRef]
15. Fan, H.; Fu, X.; Zhang, Z.; Wu, Q. Phenology-based vegetation index differencing for mapping of rubber plantations using Landsat OLI data. *Remote Sens.* **2015**, *7*, 6041–6058. [CrossRef]
16. Le, Yu; Liang, L.; Wang, J.; Zhao, Y.Y.; Cheng, Q.; Hu, L.Y.; Liu, S.; Yu, L.; Wang, X.Y.; Zhu, P.; et al. Meta-discoveries from a synthesis of satellite-based land-cover mapping research. *Int. J. Remote Sens.* **2014**, *35*, 4573–4588.
17. Zhang, W.; Li, A.; Jin, H.; Bian, J.; Zhang, Z.; Lei, G.; Qin, Z.; Huang, C. An enhanced spatial and temporal data fusion model for fusing Landsat and MODIS surface reflectance to generate high temporal Landsat-like data. *Remote Sens.* **2013**, *5*, 5346–5368. [CrossRef]
18. Hu, Q.; Wu, W.; Song, Q.; Lu, M.; Chen, D.; Yu, Q.; Tang, H. How do temporal and spectral features matter in crop classification. *J. Integr. Agric.* **2017**, *16*, 324–336. [CrossRef]
19. Immitzer, M.; Vuolo, F.; Atzberger, C. First experience with Sentinel-2 data for crop and tree species classifications in central Europe. *Remote Sens.* **2016**, *8*, 166. [CrossRef]
20. Mansaray, L.; Huang, W.; Zhang, D.; Huang, J.; Li, J. Mapping rice fields in urban Shanghai, Southeast China, using Sentinel-1a and Landsat 8 datasets. *Remote Sens.* **2017**, *9*, 257. [CrossRef]

21. Jia, K.; Liang, S.L.; Gu, X.F.; Baret, F.; Wei, X.Q.; Wang, X.X.; Yao, Y.J.; Yang, L.Q.; Li, Y.W. Fractional vegetation cover estimation algorithm for Chinese GF-1 wide field view data. *Remote Sens. Environ.* **2016**, *177*, 184–191. [CrossRef]
22. Song, Q.; Zhou, Q.; Wu, W.; Hu, Q.; Lu, M.; Liu, S. Mapping regional cropping patterns by using GF-1 WFV sensor data. *J. Integr. Agric.* **2017**, *16*, 337–347. [CrossRef]
23. Kong, F.; Li, X.; Wang, H.; Xie, D.; Li, X.; Bai, Y. Land cover classification based on fused data from GF-1 and MODIS NDVI time series. *Remote Sens.* **2016**, *8*, 741. [CrossRef]
24. Wang, Q.; Shi, W.; Li, Z.; Atkinson, P.M. Fusion of Sentinel-2 images. *Remote Sens. Environ.* **2016**, *187*, 241–252. [CrossRef]
25. Lebourgeois, V.; Dupuy, S.; Vintrou, É.; Ameline, M.; Butler, S.; Bégué, A. A combined random forest and OBIA classification scheme for mapping smallholder agriculture at different nomenclature levels using multisource data (simulated Sentinel-2 time series, VHRS and DEM). *Remote Sens.* **2017**, *9*, 259. [CrossRef]
26. Wu, M.; Zhang, X.; Huang, W.; Niu, Z.; Wang, C.; Li, W.; Hao, P. Reconstruction of daily 30 m data from HJ CCD, GF-1 WFV, Landsat, and MODIS data for crop monitoring. *Remote Sens.* **2015**, *7*, 16293–16314. [CrossRef]
27. Hu, Q.; Wu, W.B.; Xia, T.; Yu, Q.Y.; Yang, P.; Li, Z.G.; Song, Q. Exploring the use of google earth imagery and object-based methods in land use/cover mapping. *Remote Sens.* **2013**, *5*, 6026–6042. [CrossRef]
28. Li, Q.; Wang, C.; Zhang, B.; Lu, L. Object-based crop classification with Landsat-MODIS enhanced time-series data. *Remote Sens.* **2015**, *7*, 16091–16107. [CrossRef]
29. Costa, H.; Carrão, H.; Bação, F.; Caetano, M. Combining per-pixel and object-based classifications for mapping land cover over large areas. *Int. J. Remote Sens.* **2014**, *35*, 738–753. [CrossRef]
30. Han, N.; Du, H.; Zhou, G.; Sun, X.; Ge, H.; Xu, X. Object-based classification using SPOT-5 imagery for Moso bamboo forest mapping. *Int. J. Remote Sens.* **2014**, *35*, 1126–1142. [CrossRef]
31. Castillejo-González, I.L.; López-Granados, F.; García-Ferrer, A.; Peña-Barragán, J.M.; Jurado-Expósito, M.; de la Orden, M.S.; González-Audicana, M. Object- and pixel-based analysis for mapping crops and their agro-environmental associated measures using QuickBird imagery. *Comput. Electron. Agric.* **2009**, *68*, 207–215. [CrossRef]
32. Ursani, A.A.; Kpalma, K.; Lelong, C.C.D.; Ronsin, J. Fusion of textural and spectral information for tree crop and other agricultural cover mapping with very-high resolution satellite images. *IEEE J. Sel. Top. Appl. Earth Obs.* **2012**, *5*, 225–235. [CrossRef]
33. Zhang, H.X.; Li, Q.Z.; Liu, J.G.; Du, X.; Dong, T.F.; McNairn, H.; Champagne., C.; Liu, M.X.; Shang, J.L. Object-based crop classification using multi- temporal SPOT-5 imagery and textural features with a random forest classifier. *Geocarto Int.* **2017**, 1–19. [CrossRef]
34. Breiman, L. Random forests. *Mach. Learn.* **2001**, *45*, 5–32. [CrossRef]
35. Mathur, A.; Foody, G.M. Crop classification by support vector machine with intelligently selected training data for an operational application. *Int. J. Remote Sens.* **2008**, *29*, 2227–2240. [CrossRef]
36. Tatsumi, K.; Yamashiki, Y.; Canales Torres, M.A.; Taipe, C.L.R. Crop classification of upland fields using Random forest of time-series Landsat 7 ETM+ data. *Comput. Electron. Agric.* **2015**, *115*, 171–179. [CrossRef]
37. Ok, A.O.; Akar, O.; Gungor, O. Evaluation of random forest method for agricultural crop classification. *Eur. J. Remote Sens.* **2012**, *45*, 421–432. [CrossRef]
38. Fletcher, R.S. Using vegetation indices as input into random forest for soybean and weed classification. *Am. J. Plant Sci.* **2016**, *7*, 2186–2198. [CrossRef]
39. Sonobe, R.; Tani, H.; Wang, X.; Kobayashi, N.; Shimamura, H. Parameter tuning in the support vector machine and random forest and their performances in cross- and same-year crop classification using TerraSAR-X. *Int. J. Remote Sens.* **2012**, *35*, 260–267. [CrossRef]
40. Duro, D.C.; Franklin, S.E.; Dubé, M.G. A comparison of pixel-based and object-based image analysis with selected machine learning algorithms for the classification of agricultural landscapes using SPOT-5 HRG imagery. *Remote Sens. Environ.* **2012**, *118*, 259–272. [CrossRef]
41. Duro, D.C.; Franklin, S.E.; Dubé, M.G. Multi-scale object-based image analysis and feature selection of multi-sensor earth observation imagery using random forests. *Int. J. Remote Sens.* **2012**, *33*, 4502–4526. [CrossRef]

42. Vieira, M.A.; Formaggio, A.R.; Rennó, C.D.; Atzberger, C.; Aguiar, D.A.; Mello, M.P. Object based image analysis and data mining applied to a remotely sensed Landsat time-series to map sugarcane over large areas. *Remote Sens. Environ.* **2012**, *123*, 553–562. [CrossRef]
43. Bureau, H.S. *Heilongjiang Statistic Yearbook*; Bureau of Heilongjiang Statistic: Harbin, China, 2015.
44. China Centre for Resources Satellite Data and Application. Available online: http://www.cresda.com/CN/ (accessed on 17 December 2014).
45. Baatz, M.; Schäpe, A. Multiresolution segmentation: An optimization approach for high quality multi-scale image segmentation. *J. Photogramm. Remote Sens.* **2000**, *58*, 12–23.
46. Mathieu, R.; Aryal, J.; Chong, A.K. Object-based classification of Ikonos imagery for mapping large-scale vegetation communities in urban areas. *Sensors* **2007**, *7*, 2860–2880. [CrossRef] [PubMed]
47. Drăguţ, L.; Tiede, D.; Levick, S.R. ESP: A tool to estimate scale parameter for multiresolution image segmentation of remotely sensed data. *Int. J. Geogr. Inf. Sci.* **2010**, *24*, 859–871. [CrossRef]
48. Jia, K.; Wu, B.; Li, Q. Crop classification using HJ satellite multispectral data in the North China Plain. *J. Appl. Remote Sens.* **2013**, *7*, 073576. [CrossRef]
49. Zhong, L.; Gong, P.; Biging, G.S. Efficient corn and soybean mapping with temporal extendability: A multi-year experiment using Landsat imagery. *Remote Sens. Environ.* **2014**, *140*, 1–13. [CrossRef]
50. Patil, A.; Lalitha, Y.S. Classification of crops using FCM segmentation and texture, color feature. *Int. J. Adv. Res. Comput. Commun. Eng.* **2012**, *1*, 371–377.
51. Gao, T.; Zhu, J.; Zheng, X.; Shang, G.; Huang, L.; Wu, S. Mapping spatial distribution of larch plantations from multi-seasonal Landsat-8 OLI imagery and multi-scale textures using Random Forests. *Remote Sens.* **2015**, *7*, 1702–1720. [CrossRef]
52. Pelletier, C.; Valero, S.; Inglada, J.; Champion, N.; Dedieu, G. Assessing the robustness of Random Forests to map land cover with high resolution satellite image time series over large areas. *Remote Sens. Environ.* **2016**, *187*, 156–168. [CrossRef]
53. Peña, M.A.; Brenning, A. Assessing fruit-tree crop classification from Landsat-8 time series for the Maipo Valley, Chile. *Remote Sens. Environ.* **2015**, *171*, 234–244. [CrossRef]
54. Loosvelt, L.; Peters, J.; Skriver, H.; Lievens, H.; Coillie, F. Random forests as a tool for estimating uncertainty at pixel-level in SAR image classification. *Int. J. Appl. Earth Obs.* **2012**, *19*, 173–184. [CrossRef]
55. Maus, V.; Camara, G.; Cartaxo, R.; Sanchez, A.; Ramos, F.M. A time-weighted dynamic time warping method for land-use and land-cover mapping. *IEEE J. Sel. Top. Appl. Earth Obs.* **2016**, *9*, 1–11. [CrossRef]
56. Petitjean, F.; Inglada, J.; Gancarski, P. Satellite image time series analysis under time warping. *IEEE Trans. Geosci. Remote Sens.* **2012**, *50*, 3081–3095. [CrossRef]
57. Petitjean, F.; Kurtz, C.; Passat, N.; Arski, P.G. Spatio-temporal reasoning for the classification of satellite image time series. *Pattern Recogn. Lett.* **2012**, *33*, 1805–1815. [CrossRef]
58. Waldner, F.; Canto, G.S.; Defourny, P. Automated annual cropland mapping using knowledge-based temporal features. *ISPRS J. Photogramm. Remote Sens.* **2015**, *110*, 1–13. [CrossRef]
59. Yan, L.; Roy, D.P. Automated crop field extraction from multi-temporal web enabled Landsat data. *Remote Sens. Environ.* **2014**, *114*, 42–64. [CrossRef]
60. Böck, S.; Immitzer, M.; Atzberger, C. On the objectivity of the objective function–problems with unsupervised segmentation evaluation based on global score and a possible remedy. *Remote Sens.* **2017**, *9*, 769. [CrossRef]